GEOPHYSICAL TRANSACTIONS 1993
Vol. 38. No. 2-3. pp. 167-189

BEHAVIOUR OF SP LOG IN A GRANITE RESERVOIR

Ali Belgasem BOURIMA *

Spontaneous potential (SP) curves generally do not show clear responses in most igneous rocks since these rocks do not possess the electrochemical activities required to generate SP anomalies.

In other cases, however, the mineralogical structure of igneous rocks is accompanied by rich development of electrochemically active minerals, such as clay minerals, zeolites, and pyrite. In these cases significant SP anomalies can be recorded. In the Nafoora-Augila field of the Sirte basin, Libya, such SP anomalies were recorded in a granite reservoir. These anomalies are investigated and the related geochemical and hydraulic background is revealed. Accordingly, theoretical petrophysical models were elaborated based on the contribution of electromotive forces generated by eletrochemically active minerals as well as on the contribution of fractures.

Keywords: SP anomalies, positive anomalies, negative anomalies, granite reservoir, fractures

1. Introduction

Shales are mixtures of various clay minerals, which are generally composed of silicon, aluminium, and oxygen. The most common clay mineral in granite is chlorite, which develops as a result of hydrothermal alteration of biotite, and kaolinite as a result of hydrothermal alteration of alkali feldspars. All clay minerals have one feature in common: their crystalline structure is dominated by tetrahedral disposition of the silicon and oxygen atoms and an octahedral arrangement of the aluminium and oxygen atoms.

The nature of the structure of the clay mineral crystals in which oxygen ions occupy the outer extremities, determines the net negative charge on the lattice [SERRA 1986].

* The Libyan National Oil Corporation (NOC), Joint Venture Dep. Elsyadi street, Tripoli, Libya
Current address: Geophysical Department, Eötvös Loránd University (ELTE), H-1083 Budapest, Ludovika tér 2.
Manuscript recevied: 4 March, 1992

The resulting negative charge loosely binds the cations to clay and repulses the anions. In effect, a clay bed acts as an ion sieve allowing only cations to permeate or pass through its structure. This property gives rise to the clay potential [HELANDER 1983].

If the water of formation is more saline than the mud, a larger number of ions from the formation water than from the mud will move into the clay. The net effect will be a flow of cations (+) through the clay to the mud.

Because of the predominantly excess negative charges of the clay framework, anions cannot migrate in the same way so each cation transferred from the formation water to the mud leaves a negative charge behind in the formation water and adds a positive charge to the mud. This accumulation of charges makes the electrical potential of the formation water more negative and that of the mud more positive. This potential difference across the clay is then equal to the electromotive force (emf) of the cell. Zeolites are also deposited along fractures in the granite [ROBERTSON Group 1990]. They are believed to behave similarly to clay minerals with respect to their electrochemical activity. Both clay minerals and zeolites exhibit the same SP responses, namely they will show positive SP anomalies in the drilling mud when this mud is less saline than the interstitial water (i.e. in the 'normal' case).

On the other hand, metallic minerals, such as pyrite, are characterized by their dominant positive charges at their inner surfaces that are in contact with the less saline drilling mud. Hence, the electrochemical activity of pyrite is attributed to the potential difference generated by excess positive charges on pyrite which charges are, in turn, compensated by excess negative charges in the drilling mud [DAKNOV 1967]. The result is that the pyritic zones will show negative SP anomalies. The depositional manner of pyrite along the fractures governs the magnitude of the SP amplitude.

In a borehole drilled in a granite reservoir in the Nafoora-Augila field, Sirte basin (*Fig. 1*), the SP curve demonstrates a number of informative features. The granite shows complicated mineral development. The upper level of the interval is dominated by weathered granite, where orthoclase was partially or totally kaolinized. The lower part is characterized by extensive fractures of different magnitude (i.e. aperture, density, number of fractures/meter, extension). These features were the sites for precipitation of some transported minerals such as pyrite and zeolites. Chlorite developed in some zones as a result of hydrothermal alteration of biotite. Besides, some fractures are assumed to be partially or totally open.

2. Qualitative analysis of the SP anomalies

Figure 2 shows the recorded SP versus depth along with other measured logs. Quite distinctive SP features can be seen from this curve. By quick look investigation, one can attribute these anomalies to different minerals which developed within the granite.

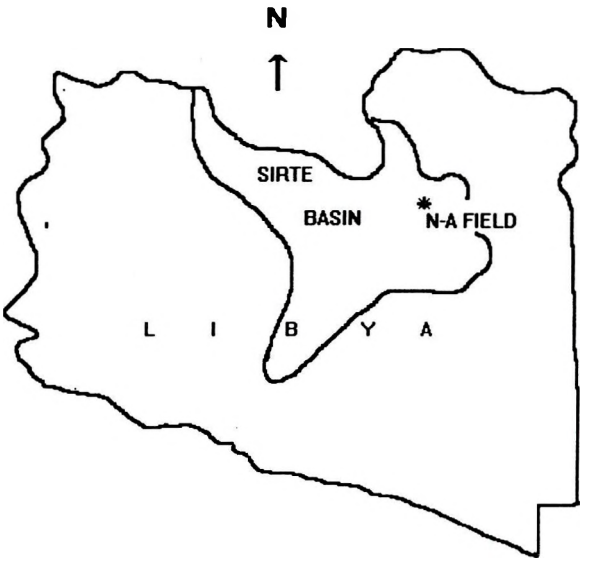

Fig. 1. Nafoora-Augila field of the Sirte Basin, Libya (not to scale)
1. ábra. Nafoora-Auglia mezõ a Sirte-medencében (nem méretarányos)

In the Nafoora-Augila borehole under investigation the mud resistivity (R_m) is equal to 0.375 Ωm at bottom-hole temperature (BHT), while the formation-water resistivity (R_w) is about 0.0178 Ωm. This means R_m is greater than R_w by more than twenty-one times, which is quite favourable for the development of SP anomalies of electrochemical nature in the granite.

There are four main electrochemically active minerals within the granite body in this borehole. They include clay minerals (i.e. kaolinite and chlorite), zeolite minerals, and pyrite. These minerals can be classified into two groups on the basis of electrochemical activity:

— electrochemically positive minerals: i.e. kaolinite, chlorite, and zeolites;
— electrochemically negative minerals: i.e. pyrite.

The SP anomalies are generated by these electrochemically active minerals. However, the open fractures play only a minor role since they do not generate SP currents but contribute to the SP current flow as passive electrical conductances if they (i.e. the fractures) are filled with electrolytes, namely conductive mud and/or interstitial water.

Nuclear-type geochemical logs (Pe, formation density log ρ_b, neutron porosity log ϕ_N, and spectral gamma ray log SGR) were utilized to identify electrochemically active minerals based on the criteria explained in Appendix I. By analysing all these logs I found that the revealed zones of electrochemically active minerals are in accordance with the developed SP anomalies (Fig. 2).

Pyrite was revealed at about eleven intervals or places (Fig. 2). The SP curve exhibits good agreement with the pyritic zones, where negative anoma-

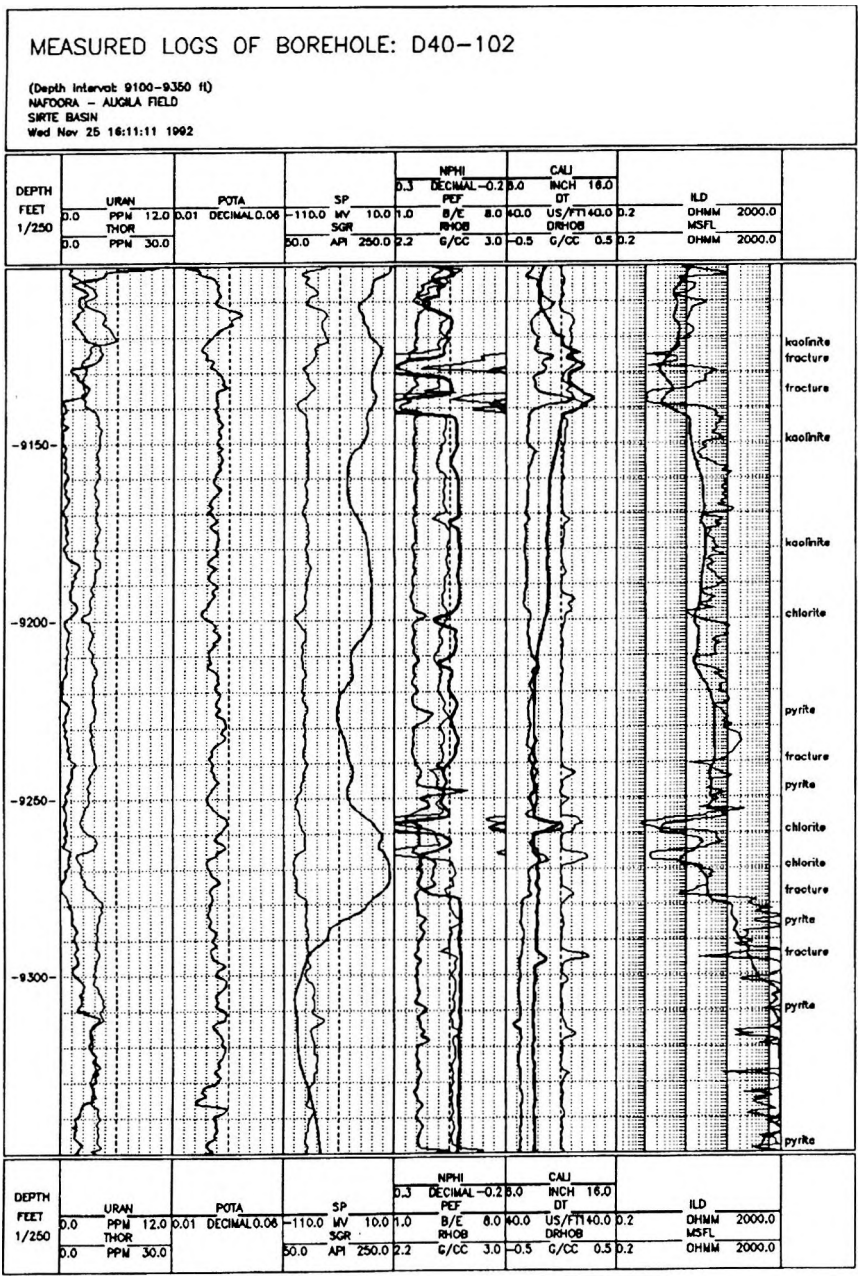

Continued on page 5

Continuation of Fig. 2.

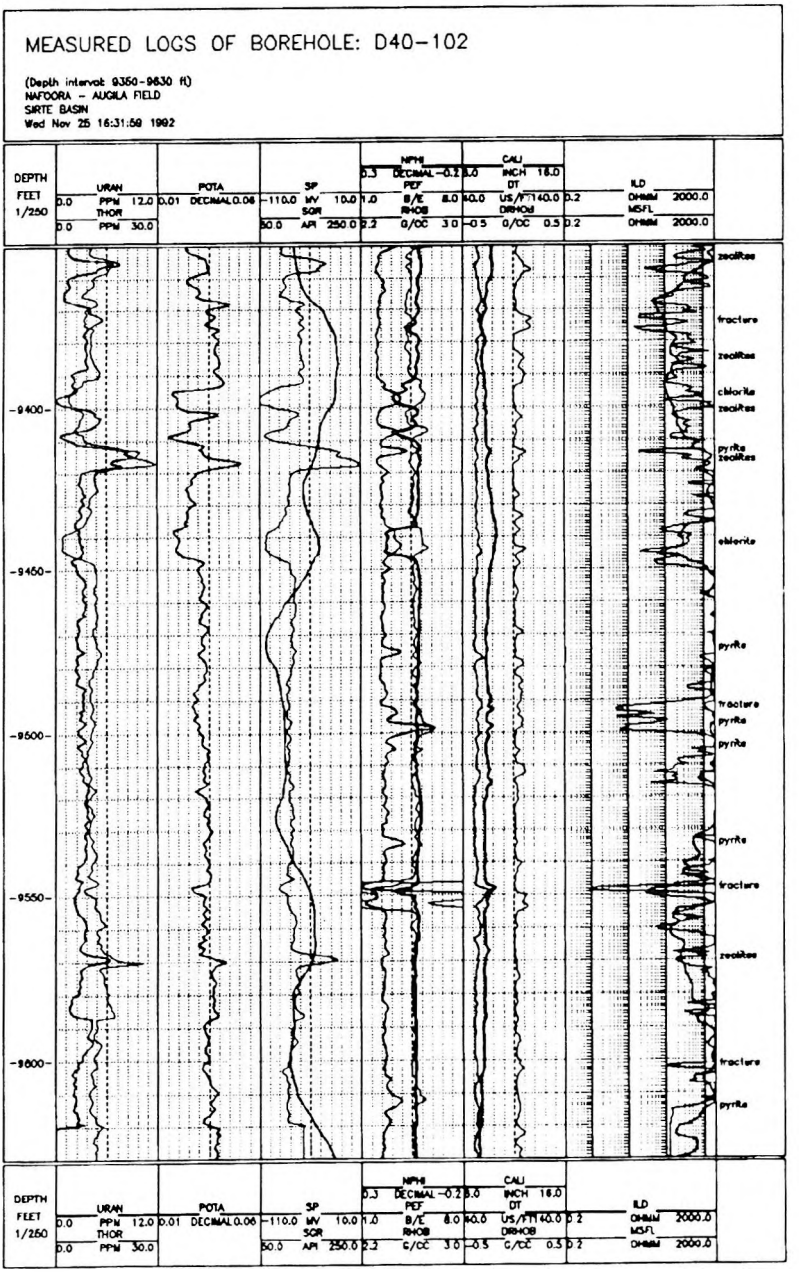

Fig. 2. Recorded SP log along with other measured logs in the granite studied

2. ábra. Mért SP szelvény, a tanulmányozott gránitban felvett egyéb szelvényekkel

lies were recorded. Chloritic zones were assumed to be developed at about six sites, and the SP represented these zones by positive excursions. The same is the case with respect to zeolitic zones, where the SP responded with positive anomalies (Fig. 2, *Fig. 3*). At the upper interval indicated in Fig. 2, kaolinite-rich places also responded with positive SP anomalies.

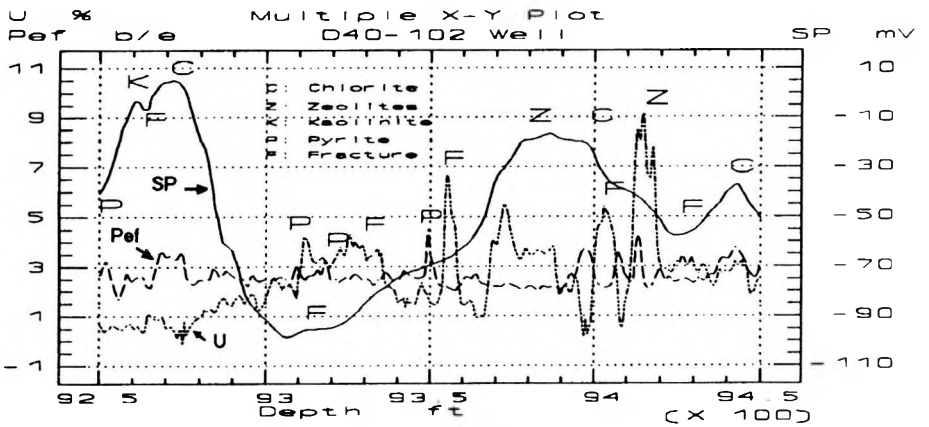

Fig. 3. SP, Pef and U logs of depth interval 9250-9450 ft (2819-2880 m) of well D40-102 showing the general relationships between the SP curve, Pef and U logs responses to electrochemicaly active minerals as well as fractures

3. ábra. A 9250-9450 ft (2819-2880 m) mélységintervallum SP, Pef és U szelvényei a D40-102 fúrólyukban, általános összefüggéseket mutatnak az SP, Pef és U szelvényeknek az elektrokémiailag aktív ásványokra és a repedezettségekre adott válaszaikra

Figure 4 is a multi crossplot representing relations of thorium versus photoelectric cross section index and potassium logs as well as K-40 versus Pef and Th. All the possible fractures, open and partially or totally blocked were detected by combined application of the Micro Spherically Focused Resistivity log (MSFL) and the geochemical logs that will be explained later. All the nuclear logs were affected by a rugosity problem at the same places to different degrees. For this reason, it was rather difficult to identify the kind of minerals within these places. However, the SP curve was helpful as a means of recognizing these minerals. Chlorite was the most probable mineral to be developed within the rugose zones since positive SP anomalies were observed here.

One of the major tasks of well log analysis in granite is to reveal the hydraulically open fractures and to distinguish them from the closed ones. I analysed the possible contribution of the SP log to this challenging problem when there are no electrokinetic SP anomalies generated in the open permeable fractures as is the case in this borehole (Fig. 3 and *Fig. 5*). The open fractures serve as passive conductors, they will modify only the shape of the electrochem-

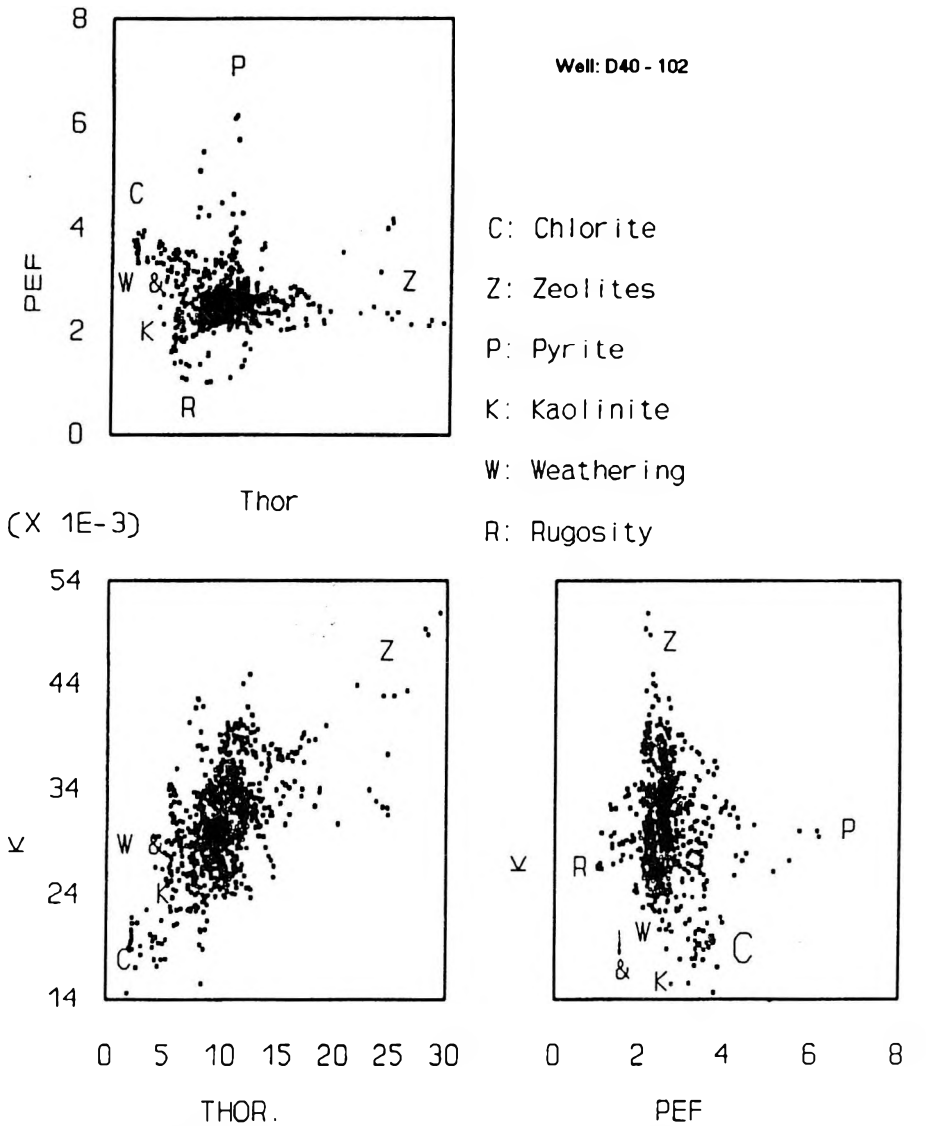

Fig. 4. Multicrossplot representing relations of thorium (Th), versus photoelectric cross section index (Pef), and potassium (K-40), measurements; as well as K-40 versus Pef and Th measurements

4. ábra. Többszörös korreláció a tórium (Th), a fotoelektromos keresztszelvény index (Pef), és a kálium (K-40) mérések adatai; továbbá a K-40 és a Pef valamint Th mérések között

ical anomalies by providing a current path from the rock to the borehole or vice versa, the open fractures create positive or negative curvatures on the SP log which are superimposed on the negative or positive local SP anomalies caused by electrochemically active solid minerals.

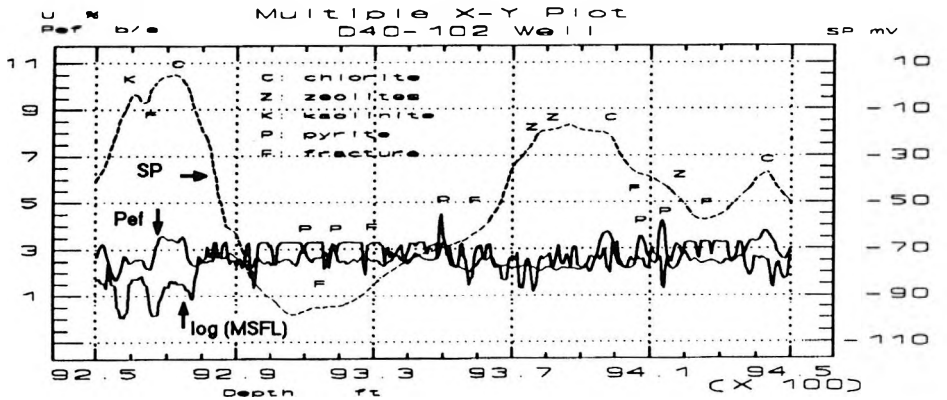

Fig. 5. SP, Pef and log(MSFL) of depth interval 9250-9450 ft (2819-2880 m) of D40-102 well showing the general relationship between the SP, Pef and MSFL logs responses to electrochemically active minerals as well as fractures

5. ábra. A 9250-9450 ft (2819-2880 m) mélységintervallum SP, Pef és log(MSFL) szelvényei, a D40-102 fúrólyukban, általános összefüggéseket mutatnak az SP, Pef és MSFL szelvényeknek az elektrokémiailag aktív ásványokra és a repedezettségekre adott válaszaikra

One can conclude that the positive and negative curvatures on the SP logs which cannot be attributed to electrochemically active minerals are facing open fractures, accordingly they (i.e. negative and positive curvatures on SP logs) can indicate the sites of open fractures. Generally, fractured places are mainly located adjacent to hydrothermally altered zones which are clearly shown by SP curves (Figs. 2, 3 and 5, where some fractured sites are indicated).

3. Petrophysical models for the SP observations in the granite reservoir

Petrophysical models for the SP observations in granite are simply based on the fact that granite reservoir body includes some electrochemically active minerals. These minerals are distributed along the total interval. The SP anomalies are real reflections for these active electrochemical minerals because they are responsible for generating the SP electromotive forces. However, fractured zones and possibly permeable vuggy zones contribute only as passive conductors to the SP field. For this reason, fracture sites sometimes do not show significant correlation with the SP anomalies [BOURIMA 1993].

Figure 6 shows a model for simulating SP excursions. It is composed of pyritic active zone, hard granite, a chloritic zone of low concentration, fractured granite, and a chloritic active zone of relatively high concentration of chlorite.

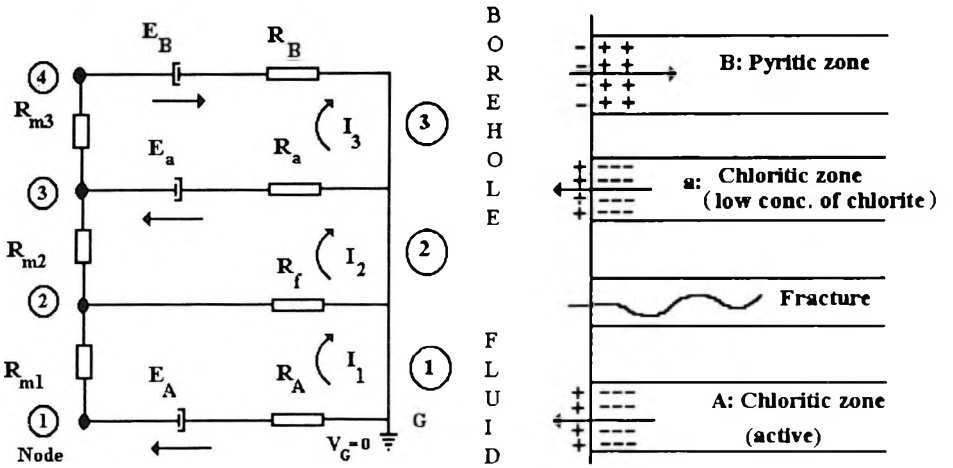

Fig. 6. Simple model composed of pyritic active zone, chloritic zone of low concentration, fractured granite, and active chloritic zone (right side) and related analog electrical network (left side). *E*—electromotive force; *I*—loop current; R_m—mud resistivity; *R*—resistivity of the rock zone

6. ábra. Aktív pirites zónából, alacsony koncentrációjú zónából, repedezett gránitból és aktív kloritos zónából felépített egyszerű modell (jobb oldalon), valamint a hozzá tartozó analóg elektromos hálózat (bal oldalon). *E*—elektromotoros erő; *I*— a hurokbani áram; R_m—fajlagos iszapellenállás; *R*—a kőzetzóna fajlagos ellenállása

The rock model of Fig. 6 is associated with the related analog electric network. This electric network is composed of a chain-structure of π-shaped cells which contain active electromotive forces, and passive resistances. The electromotive forces simulate the electrochemically active minerals such as pyrite, chlorite, zeolites and kaolinite. The fractures, as passive electrical conductances, are also taken into account. The electrical network also includes the mud column and the rock zones in the form of passive resistances. The presented network can be extended as far as the simulated rock components extend.

The analog network in Fig. 6 comprises three independent network loops: 1, 2, and 3. Loop currents I_1, I_2 and I_3 are attributed to each loop, respectively, indicating also the expected positive direction of the loop currents. The active emf's are also included with their positive direction from the negative to the positive side of the active electric sources. The network is mathematically treated by means of the so-called loop voltage equations including the passive ohmic potential drops along the resistivities on the left side, and the active emf's on the right side of the equations:

$$I_1 (R_A + R_{m1} + R_f) + I_2 (R_f) = E_A \tag{1}$$

$$I_1 (-R_f) + I_2 (R_f + R_{m2} + R_a) + I_3 (-R_a) = -E_a \tag{2}$$

$$I_2 (R_a) + I_3 (R_a + R_{m3} + R_B) = E_B + E_a \tag{3}$$

By assuming all the included resistivities and the electromotive forces are known quantities, Eqs. (1), (2), and (3) can be solved by common mathematical rules in order to find out the three unknowns: I_1, I_2, and I_3.

Accordingly:

$$D = (R_A + R_{m1} + R_f)[R_a^2 - (R_f + R_{m2} + R_a)(R_a + R_{m3} + R_B)] + \\ + R_f^2 (R_a + R_{m3} + R_B) \tag{4}$$

$$D_1 = E_A[R_a^2 - (R_f + R_{m2} + R_a)(R_a + R_{m3} + R_B)] + \\ + R_f [E_a (R_a + R_{m3} + R_B) - R_a (E_B + E_a)] \tag{5}$$

$$D_2 = (R_A + R_{m1} + R_f)[E_a (R_a + R_{m3} + R_B) - R_a (E_B + E_a)] - \\ - E_A R_f (R_a + R_{m3} + R_B) \tag{6}$$

$$D_3 = (R_A + R_{m1} + R_f)[E_a R_a - (E_B + E_a)(R_f + R_{m2} + R_a)] + \\ + R_f^2 (E_B + E_a) - E_A R_f R_a \tag{7}$$

Hence, the solution of the three unknowns can be obtained from these relations:

$$I_1 = \frac{D_1}{D} \tag{8}$$

$$I_2 = \frac{D_2}{D} \tag{9}$$

$$I_3 = \frac{D_3}{D} \tag{10}$$

Moreover, the voltage at the indicated nodes: 1, 2, 3 and 4 can be simply given by:

$$V_1 = -I_1 R_A + E_A \tag{11}$$

$$V_2 = V_1 - I_1 R_{m1} \tag{12}$$

$$V_3 = V_2 - I_2 R_{m2} \tag{13}$$

$$V_4 = V_3 - I_3 R_{m3} \tag{14}$$

Theoretically, the SP current enters the pyritic zone from the mud and leaves the chloritic zone into the mud column. The open fracture will be a possible path for the currents generated in the electrochemical cells. The mud column will also provide passive electrical conductances for the generated currents.

It has been proven by numerical values for the analog electric network (Appendix 2) that the SP voltage will give always distinct values for electrochemically active minerals. However, if a fracture site is located between two active mineral zones of different charges, the SP curve will show a reading lying not far from the straight line which connects the two active zones. The SP reading of the fracture shapes a positive curvature. The sharpness of this curvature is governed by the number of components in the electric network. *Figure 7* shows an example of numerical values for Fig. 6. The two curves represent the same parameters, with the exception of the fracture aperture which has been considerably increased. The right side curve is shifted to the right because of the larger width of fracture aperture, and the fracture is indicated by a stronger curvature. We can see that when the open fractures are located

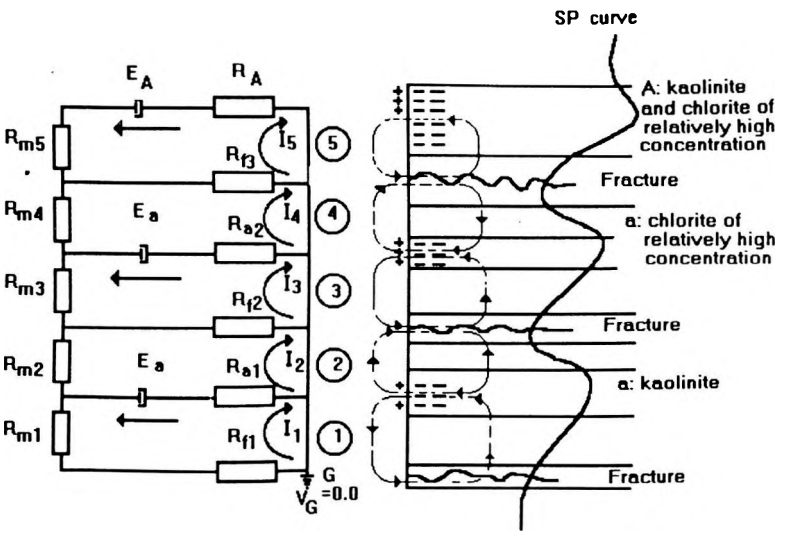

Fig. 7. Numerical calculations of the SP anomalies generated by the electrochemically active minerals and fractures presented in the model of Fig. 6

7. ábra. A 6. ábra modelljében szereplő kőzetrepedés és az elektrokémiailag aktív ásványok által előállított SP anomáliák numerikus számítása

between mineralized zones of different electrochemical nature, the SP curve alone will generally not help much in identifying the open fractures.

Figure 8 is a model simulating the SP curve recorded within the interval 9120-9160 ft (2780-2792 m). Relatively positive anomalies were recorded at three different levels of chloritic and kaolinitic zones. However, in between, two negative anomalies can be seen on the SP curve caused by open fractures. In this case the SP log is useful for detecting the open fractures. From the nuclear-type geochemical logs, there was no indication of developments of electrochemically active minerals of negative SP anomalies, such as pyrite at high concentration. This means that the recorded negative SP anomalies were not generated by any active minerals. A possible explanation of these two SP negative anomalies is provided by open fractures as presented by the petrophysical model.

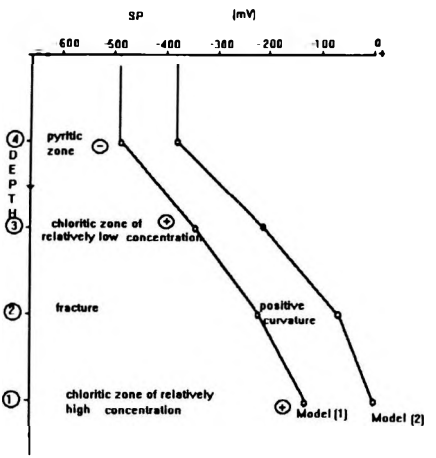

Fig. 8. Model simulating the SP curve recorded within the depth interval 9120-9160 ft (2780-2792 m). The related analog electrical network is shown on the left side

8. ábra. A 9120-9160ft (2780-2792 m) mélységintervallumban felvett SP görbét szimuláló modell. A kozzá tartozó analóg elektromos hálózat a bal oldalon látható

In the depth interval 9437.5-9549.5 ft (2876.5-2910.7 m) (*Fig. 9*) the SP curve responded to electrochemically positive chlorite at both the top and the bottom of the interval. Two negative electrochemically active zones (pyrite) were reflected by the SP curve at two separate sites that are adjacent to the indicated chloritic zones. Meanwhile in the middle of this interval the SP curve as well as the nuclear-type geochemical logs indicate a combined development of pyrite and zeolites. In this particular interval heavy fractures were assumed to be partly filled with pyrite, partly with zeolites, as a result of hydrothermal alterations. In Fig. 9 the petrophysical model (Appendix 3) to the depth interval can be seen; the measured SP curve is demonstrated at the upper part of this figure, the curve represents the estimated theoretical SP curve obtained by substituting optimized parameters for the lower analog electrical network.

Because of the complexity of this petrophysical model, where the number of the unknown loop currents is rather large, it is tedious to obtain a theoretical curve of close values to the measured one. Accordingly, a computer optimiza-

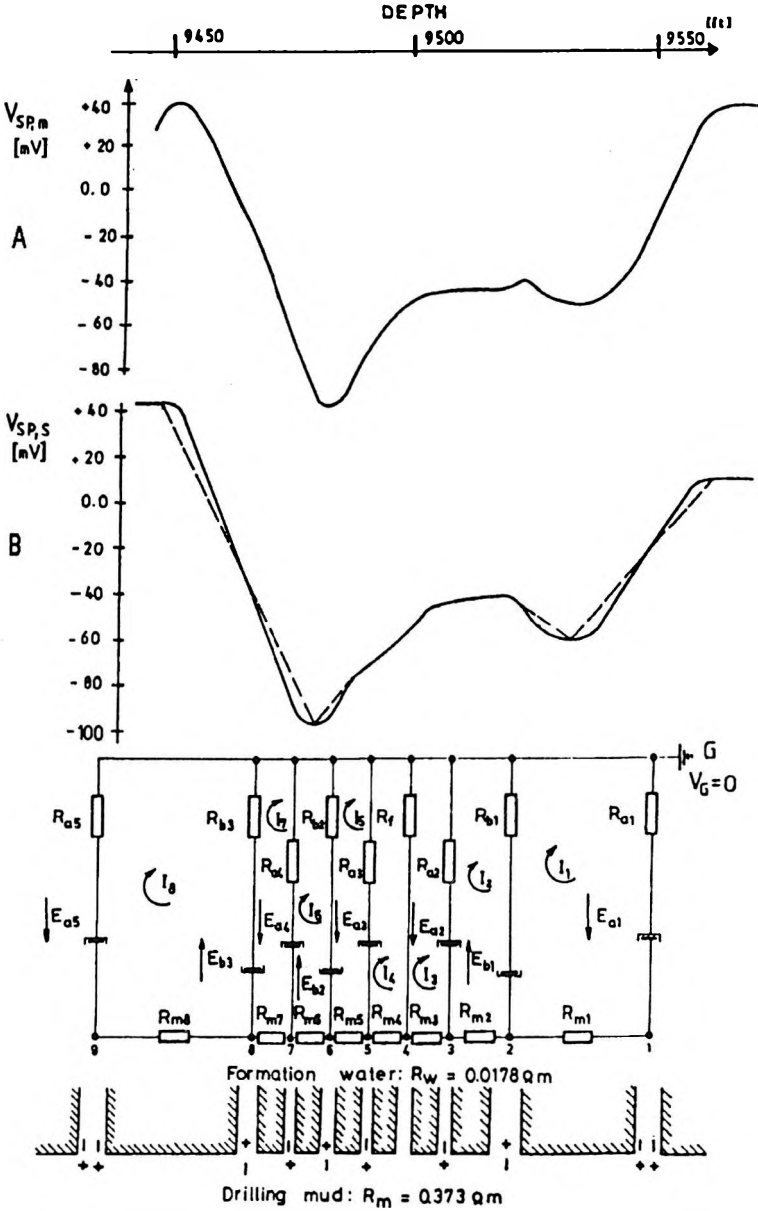

Fig. 9. SP curves and the analog electrical network of the petrophysical model. A—SP curve measured in the depth interval 9437.5-9549.5 ft (2876.5-2910.7 m) ($V_{SP,m}$); B—estimated SP curve with optimazed parameters of the network ($V_{SP,S}$)

9. ábra. Kőzettani modell SP görbéje és analóg elektromos hálózata. A—9437,5-9549,5 ft (2876,5-2910,7 m) mélységintervallumban mért SP görbe ($V_{SP,m}$); B—a hálózat optimalizált paramétereivel becsült SP görbe ($V_{SP,S}$)

tion technique is recommended for similarly detailed and complicated models in order to obtain greater accuracy.

4. Conclusions

The granite oil reservoir investigated here represents considerably useful SP excursions; these are mainly of electrochemical nature, where electrochemically active minerals, such as chlorite, kaolinite, zeolites and pyrite are the main minerals responsible for the SP anomalies. Both the nuclear-type geochemical logs and the SP log are correlated to indicate the electrochemically active minerals. In spite of the fact that the SP log does not show a distinct correlation with fracture sites, it is useful as a means of recognizing the possible fractures, particularly the open ones, along with other logs.

It has been found that the open fractures serve only as passive conductors. Because they cannot generate electrochemical emf's, they will only modify the shape of the electrochemical anomalies by providing a current path from the rock to the borehole or vice versa.

These petrophysical models and the related analog electrical network model offer a powerful technique for revealing the petrochemical and petrophysical background of the SP anomalies in the granite. In addition, these models are helpful in demonstrating the role of the open fractures in the SP excursions.

The proposed analog electric network calculations indicate that the SP will give distinctive extreme values for the emf's of electrochemically active minerals. However, if a fracture is located between two active zones of different electrical polarities, the SP curve will show readings lying not far from the straight line connecting the two active zones. At the same time, the SP log responds in a more clear manner to fractures located between two mineralized zones of the same electrochemical nature.

Acknowledgements

The author would like to thank the Libyan National Oil Corporation (NOC), for making the data for this work available. My great thanks are also due to Prof. Zoltán BARLAI for his helpful directives and constructive criticism during the analysis and writing-up of this paper. Sincere thanks are also expressed to Prof. Attila MESKÓ, head of the Geophysical Department of Eötvös Loránd University, Budapest, and Dr. Dezső DRAHOS for their help and support. This work is sponsored in part by the Libyan National Oil Corporation.

REFERENCES

BOURIMA A. B. 1993: New Synergetic Approach for An Oil-bearing Granite Reservoir Evaluation by Means of Well Logs, Ph.D. thesis, Hungarian Academy of Sciences, MTA, 1993, pp. 52-78

CLAVIER C., HEIM A., SCALA C. 1976: Effect of pyrite on resistivity and other logging measurements. Paper HH, in the 17th Annual Logging Symposium Transactions: SPWLA, 1976, pp. 1-34

CLIFTON R. 1986: Natural and Synthetic zeolites, United States of the Interior Bureau of Mines, pp. 2-10

DAKNOV V. N. 1967: Electrical and magnetic methods of investigation of boreholes; Fundamentals of theory (in Russian), Published by Nedra, Moscow, 1967, pp. 345-348

HELANDER D. P. 1983: Fundamentals of formation evaluation. OGCI Publications, pp. 77-97

JUDSON S., KAUFFMAN M. E. 1990: Physical Geology, Eighth Edition, Prentice Hall Englewood Cliffs, New Jersey, pp. 39-133

The Rebortson Group plc, 1990: Reservoir description and petrophysical study of the Nafoora-Augila Unit, Report prepared for The Arabian Gulf Oil Company, 1990.

SERRA 1986: Fundamentals of well interpretation (part one). Elsevier, Amsterdam

APPENDIX 1

THE MAIN SECONDARY MINERALS IDENTIFIED AND THE CRITERIA USED FOR THEIR DISCRIMINATION

KAOLINITE

Kaolinite is one of the main clay minerals. It is a hydrous aluminous silicate $Al_4(Si_4O_{10})(OH)_8$. The structure consists of one sheet of silicon-oxygen tetrahedron each of which shares three oxygens to give the ratio of $(Si_4O_{10})^{4-}$ linked with one sheet of aluminum hydroxyl.

The igneous rocks of the Nafoora-Augila field were affected by a diagenetic process where in certain parts of rock a series of transformations had taken place. Kaolinite was developed mainly in the weathered parts and possibly within fractures, brecciation and leached feldspar pores as a result of hydrothermal alteration of potassium feldspars.

Because of the weathering process that results in the development of kaolinite, Th, U, and K-40 were leached out from the affected zones. Thus, the spectral gamma ray logs generally show low values at these levels. On the other hand, neutron porosity shows increased values in such zones due to the hydrous structure of kaolinite and a possible increase in the total porosity, partly due to the created

unblocked part of fractures and/or vugs. However, it should be mentioned that the neutron porosity tools (CNL) are calibrated in limestone rock and different versions have some differences with respect to different rock matrix responses.

Lithodensity logs, ρ_b and Pef, exhibit comparatively low values in response to kaolinite, however, they are not conspicuous enough to be used as an indicator for kaolinite accumulation.

The SP log is an important indicator showing positive SP anomalies for the existence of kaolinitic zones within the granite, where it is not easy to identify them by other geophysical well logs, especially when the kaolinite developed in limited quantities.

The importance of the SP is enhanced for kaolinite identification when it existis in a dehydrated form. In this case, the neutron porosity log, which usually gives distinctive values for kaolinite, becomes useless. Nevertheless, neutron porosity as well as lithodensity logs, can be utilized to discriminate between kaolinite and chlorite, which have the same positive SP anomalies.

CHLORITE

Chlorite is a phyllosilicate of magnesium, aluminum, iron and calcium. Chlorite exhibits a cleavage similar to that of mica, but the small scales produced by the cleavage are not elastic, like those of mica [JUDSON, KAUFFMAN 1990].

In the granite of the Nafoora-Augila field, chlorite is the most dominant hydrothermally altered mineral. It is encountered in almost every weathered and non-weathered level. The chlorite is generated as a result of hydrothermal alteration of biotite. The alteration process usually takes place in fractures, breccia, faults and interconnected spaces where the circulation of fluids is possible.

Chlorite is characterized by relatively high lithodensity logs (ρ_b and Pef) and neutron porosity logs. Furthermore, chlorite exhibits postive (+) SP anomalies in the normal case. Thus, it is easy to recognize chlorite at first sight when the composite log is being investigated.

Chlorite is also conspicuously detected by natural gamma ray spectrometer logs. Chloritic zones usually exhibit considerably low gamma ray values. Evidently, the hydrothermal alteration processes are largely responsible for leaching out most of the existing radioactive host minerals.

ZEOLITES

Zeolites consist of a crystalline framework of aluminous silicates. The structure contains channels and interconnected voids occupied by cations and water molecules [CLIFTON 1987].

The development of zeolite in igneous rocks can be related to:

— zeolites precipitated in hydrothermal systems from alkaline to weakly acidic hot water. Zeolites, when they occur in deep and hot zones, are in low forms; they may be, partly or totally dehydrated.

— zeolites crystallized during the late stages of formation of magmatic rocks. They commonly occur as fine crystals lining fractures and vugs in basic igneous rocks although they also occur as interstitial particles and globules. Crystalline zeolite forms through interaction of fluids with the surrounding rock.

Aluminum-rich zeolite occurs in basic igneous rocks with low silicon-to-aluminum ratio, whereas aluminum-poor zeolite occurs in igneous rocks which are rich in silicon [CLIFTON 1987].

Zeolite and clay minerals, such as kaolinite and montmorillonite, are composed of the same chemical elements in their crystal structures. Concerning the clay minerals, with the exception of smectites, their intercrystalline and interlayer water cannot be displaced by other molecules, such as radioactive radicals, but only the outer adsorption water can be displaced. Hence, the neutron porosity log usually records high values in clay minerals. With regard to the smectites, their interlayer water can be displaced, however, because of their instability, they are not found in old rocks such as Precambrian granite.

For the reasons given, the zones indicated in Fig. 2, which are characterized by high radioactivities, are considered as zeolites in spite of their low neutron porosity values; they are usually characterized by relatively low Pef and ρ_b values which are also the cases shown by the recorded logs in Fig. 2.

The manifested absorption water contained in the interconnected void channels of zeolites is most likely displaced by potassium, thorium, and uranium which are transported from the nearby hydrothermally affected zones. Fig. 2 gives the evidence for this explanation; here the gamma ray spectral logs show erratic high values opposite the zeolitic zones. Moreover, the SP log proves the precipitation of zeolites by showing positive anomalies. This is related to the fact that zeolites are characterized by an excess of negative charges. Therefore, each counter-cation transferred from the zeolitic formation to the mud causes a positive SP potential in the mud.

PYRITE

Pyrite is a sulphide mineral, iron sulphide, FeS_2. Pyrite in granite was found lining fractures and veins. It is deposited as a result of transportation process.

Unlike the usual rock minerals, pyrite exhibits good electrical conductivity, usually comparable to or higher than the conductivity of the formation water. It is a conduction of metallic (electronic) nature and, consequently, any transfer of current between water and pyrites involves a process of conversion from ionic to electronic conduction and vice versa [CLAVIER et al. 1976]. On the other hand,

pyrite is characterized by its dominant positive charges at its inner surface, which is in contact with less saline drilling mud. Hence, the pyritic zones will show negative SP anomalies. The depositional manner of pyrite along the fractures will govern the magnitude of the SP amplitude.

Density tools exhibit an apparent density of 4.985 g/cc in pyritic zones whereas the photoelectric cross section index, Pef, indicates these zones by their high value (17 b/e). Because of these two distinctive characteristics of pyrite (high ρ_b and Pef values) it is easy to recognize pyritic zones within the granite (see Fig. 2 where pyritic zones are indicated).

The neutron porosity from limestone matrix calibration shows low values in a pyritic matrix (≈ -2%).

APPENDIX 2

Fig. 6 represents an analog electrical network composed of three independent network loops 1, 2 and 3 with loop currents I_1, I_2 and I_3 respectively. The following two examples exhibit numerical values demonstrating the role of fracture between different electrochemically active minerals in modifying the SP anomalies (See also Fig. 7);

Numerical Example 1:

$$E_A = 1.0 \text{ V} \; ; E_B = 2.0 \text{ V} \; ; E_a = 0.50 \text{ V}$$

$$R_A = R_B = 100\ \Omega \; ; \quad R_{m1} = R_{m2} = R_{m3} = 10.0\Omega$$

$$R_f = 200\ \Omega \; ; \; R_a = 300\ \Omega$$

By substituting these values into the related parameters of eqs. (4) through (14) one can obtain the following results, respectively:

$$I_1 = \frac{D_1}{D} = 0.0111 \text{ A}$$

$$I_2 = \frac{D_2}{D} = 0.0122 \text{ A}$$

$$I_3 = \frac{D_3}{D} = 0.0150 \text{ A}$$

The branch current in loop 2 will be:

$$I_1 - I_2 = -0.0011 \text{ A}$$

this means that the current will flow from the fracture to the borehole.

$$I_2 - I_3 = -0.0028 \text{ A}$$

this means that the current will flow from the chloritic zone to the borehole. The node voltages at the indicated nodes are given;

$$V_1 = -I_1 R_A + E_A = -0.1115 \text{ V}$$

$$V_2 = R_f (I_1 - I_2) = -0.2227 \text{ V}$$

$$V_3 = V_2 - I_2 R_{m2} = -0.3450 \text{ V}$$

$$V_4 = V_3 - I_3 R_{m3} = -0.4954 \text{ V}$$

Numerical Example 2:

In this example all the proposed parameter values of the previous example have been retained with only one exception, namely the fracture aperture has been increased ten-fold. Hence the related resistance decreased to the one-tenth value, i.e. to $R_f = 20\ \Omega$.

Accordingly, the calculations by means of eqs. (4) through (14) are given by the following, respectively;

$$I_1 = \frac{D_1}{D} = 0.0098 \text{ A}$$

$$I_2 = \frac{D_2}{D} = 0.0138 \text{ A}$$

$$I_3 = \frac{D_3}{D} = 0.0162 \text{ A}$$

The branch currents in loop 2 will be:

$$I_1 - I_2 = -0.0040 \text{ A}$$

this means that the current will flow from the fracture to the borehole.

$$I_2 - I_3 = -0.0024 \text{ A}$$

this means that the current will flow from the chloritic zone to the borehole. The node voltages at the indicated nodes are given by;

$$V_1 = -I_1 R_A + E_A = 0.0183 \text{ V}$$

$$V_2 = R_f (I_1 - I_2) = -0.0800 \text{ V}$$

$$V_3 = V_2 - I_2 R_{m2} = -0.2180 \text{ V}$$

$$V_4 = V_3 - I_3 R_{m3} = -0.3800 \text{ V}$$

APPENDIX 3

The petrophysical model represented by Fig. 9 is numerically evaluated here, in order to obtain a simulated SP curve which is close to the measured one. As can be seen from this figure the related analog electric network contains eight loops. More generally, a mathematical algorithm for simulating an electrical circuit consisting of K loops is suggested.

Without violating the generality of the formulation of the problem, the system of linear equations for an electric network containing K loops can be introduced by the following special band limited matrix:

$$\begin{vmatrix} -a_1 & 1 & \cdot & \cdot & \cdots & \cdot & \cdot \\ -\tilde{a_2} & -a_2 & 1 & \cdot & \cdots & \cdot & \cdot \\ \cdot & -\tilde{a_3} & -a_3 & 1 & \cdots & \cdot & \cdot \\ \cdot & \cdot & \cdot & \cdot & \cdots & \cdot & \cdot \\ \cdot & \cdot & \cdot & \cdot & \cdots & \cdot & \cdot \\ \cdot & \cdot & \cdot & \cdot & \cdots & \cdot & 1 \\ \cdot & \cdot & \cdot & \cdot & \cdots & -\tilde{a_k} & -a_k \end{vmatrix} \begin{vmatrix} I_1 \\ I_2 \\ \cdot \\ \cdot \\ \cdot \\ \cdot \\ I_k \end{vmatrix} = \begin{vmatrix} b_1 \\ b_2 \\ \cdot \\ \cdot \\ \cdot \\ \cdot \\ b_k \end{vmatrix} \tag{15}$$

where $\tilde{a_m}$ denotes the matrix elements standing only in the mth line, which is not in the main diagonal and it is not necessary for it to be equal to 0 or 1.

I_m can be expressed by using only I_{m-1}, I_{m-2} in the form;

$$I_m = b_{m-1} + a_{m-1} * I_{m-1} + \tilde{a}_{m-1} * I_{m-2} \tag{16}$$

This formula is valid when m=3, 4, 5 ... k, and after the definition of $\tilde{a}_1 = 0.0$, eq. (16) becomes valid for m=2 as well.

The strategy followed for solving the system presented by eq. (15) is as follows: We denote I_1 by X and using the 1, 2, ...(k-1)th row of the system, I_2, I_3, ... I_k are expressed in successive order and only with the aid of X. Then, the value of X can be obtained by using the kth row of equation system. Since $X=I_1$, equation (16) is now used to find the values I_2, I_3, ... I_k.

As a realization of the above described process, a definition for X, and equation (16), in the case of m=2, 3, 4, ..., is as follows:

$$I_1 = X \tag{17}$$

$$I_2 = b_1 + a_1 I_1 \tag{18}$$

$$I_3 = b_2 + a_2 I_2 + \tilde{a_2} I_1 \tag{19}$$

$$I_4 = b_3 + a_3 I_3 + \tilde{a_3} I_2 \tag{20}$$

We substitute the first eq. (17) of the system of equations (i.e the X value) into the right side of the second equation of system (18), and the new values of I_1 and I_2 (i.e. the second equation of the system), accordingly, have to be substituted into the right side of the next equation and so forth with respect to I_3, I_4 etc. This is simply given by:

$$I_1 = 0 + 1 \cdot X$$
$$I_2 = b_1 + a_1 \cdot X$$
$$I_3 = (b_2 + a_2 b_1) + (a_2 a_1 + \tilde{a_2}) \cdot X$$
$$I_4 = (b_3 + a_3 b_2 + a_3 a_2 b_1 + \tilde{a_3} b_1) + (a_3 a_2 a_1 + a_3 \tilde{a_2} + \tilde{a_3} a_1) \cdot X$$

However, the following equation represents the general term:

$$I_m = v_m + w_m \cdot X \tag{21}$$

So, as a result of the generation rule (16), it is not difficult to realize that both v_m (the constant part of I_m) and w_m (the coefficient of X), can be derived according to the sequences with non-constant coefficients as follows:

$$\begin{aligned} v_1 &= 0 \\ v_2 &= b_1 \\ &\cdot \\ &\cdot \\ &\cdot \\ &\cdot \\ v_m &= b_{m-1} + a_{m-1} \cdot v_{m-1} + \tilde{a}_{m-1} \cdot v_{m-2} \end{aligned} \tag{22}$$

$$\begin{aligned} w_1 &= 1 \\ w_2 &= a_1 \\ &\cdot \\ &\cdot \\ &\cdot \\ &\cdot \\ w_m &= a_{m-1} \cdot w_{m-1} + \tilde{a}_{m-1} \cdot w_{m-2} \end{aligned} \tag{23}$$

By substituting eq. (21), in the case of $m = k$ and $m = k-1$ into the last row of the system of eqs. (15), the result can be rearranged as follows;

$$-(a_k \cdot w_k + \tilde{a_k} \cdot w_{k-1}) \cdot X = b_k + a_k \cdot v_k + \tilde{a_k} \cdot v_{k-1} \tag{24}$$

By substituting eqs. (22) and (23), in the case of $m = k+1$, into eq. (24), the final formula is as follows:

$$X = -\frac{V_{k+1}}{W_{k+1}} \tag{25}$$

When the X becomes a known quantity, the values of $I_2, I_3, \ldots I_k$ can be obtained sequentially by means of eq. (21).

Numerical Example:

The trial and error technique is followed to determine the appropriate set of network parameters involved in the eight network equations describing the petrophysical model of Fig. 9. However, a computer optimization technique is recommended for future work in order to solve more complicated network models with efficient time and accuracy conditions. In the final stage of trial and error optimization the following set of network parameter values were obtained:

$E_{b3} = 0.60$ V, $E_{b2} = 0.15$ V, $E_{b1} = 1.00$ V, $E_{a5} = 1.2$ V

$E_{a4} = 0.15$ V, $E_{a3} = 0.45$ V, $E_{a2} = 0.35$ V, $E_{a1} = 0.3$ V

$R_{m1} = 23.70\ \Omega$, $R_{m2} = R_{m3} = R_{m4} = R_{m5} = R_{m6} = R_{m7} = 10.0\ \Omega$,

$R_f = 300.0\ \Omega$, $R_{a1} = 100.0\ \Omega$, $R_{a3} = 400.0\ \Omega$, $R_{a5} = 150.0\ \Omega$

$R_{a2} = R_{a4} = R_{b1} = R_{b2} = 200.0\ \Omega$, $R_{b3} = 50.0\ \Omega$, $R_{m8} = 18.10\ \Omega$

The above explained mathematical steps, for k=8, have been followed by using these parameter values, and finally the following results were obtained:

The loop currents are:

$I_1 = 0.0029$ A
$I_2 = -0.0018$ A
$I_3 = 0.0002$ A
$I_4 = 0.0003$ A
$I_5 = 0.0016$ A
$I_6 = 0.0012$ A
$I_7 = 0.0023$ A
$I_8 = -0.0077$ A

The branch currents are:

$I_1 - I_2 = 0.0047$ A
$I_2 - I_3 = -0.0019$ A
$I_3 - I_4 = -0.0002$ A
$I_4 - I_5 = -0.0012$ A

$I_5 - I_6 = 0.0004$ A
$I_6 - I_7 = -0.0011$ A
$I_7 - I_8 = 0.0100$ A

The node voltages at the indicated nodes are given by;

$$V_4 = R_f(I_3 - I_4) = -0.0452$$
$$V_3 = V_4 + R_{m3}I_3 = -0.0433$$
$$V_2 = V_3 + R_{m2}I_2 = -0.0611$$
$$V_1 = V_2 + R_{m1}I_1 = 0.0081$$
$$V_5 = V_4 + R_{m4}I_4 = -0.0486$$
$$V_6 = V_5 + R_{m5}I_5 = -0.0645$$
$$V_7 = V_6 + R_{m6}I_6 = -0.0761$$
$$V_8 = V_7 + R_{m7}I_7 = -0.0990$$
$$V_9 = V_8 + R_{m8}I_8 = -0.0408$$

With the optimized set of network parameters there is a fairly good agreement between the estimated SP curve and the measured one, which proves the usefulness of the above explained method.

SP SZELVÉNYEZÉS TULAJDONSÁGAI GRÁNIT TÁROZÓBAN

Ali Belgasem BOURIMA

A legtöbb magmás kőzet esetében a spontán potenciál (SP) szelvényezés válaszgörbéi nem jellegzetesek, mivel ezen kőzetek nem rendelkeznek olyan elektrokémiai aktivitással, mely szükséges az SP anomáliák létrejöttéhez. Egyes esetekben azonban, a magmás kőzet ásványos-szerkezetét elektrokémiailag aktív ásványok gazdag kifejlődése jellemzi, mint például agyagásványok, zeolitok és pirit. Ezekben az esetekben jelentős SP anomáliák rögzíthetők. A líbiai Sirte-medencében található Nafoora-Augila mezőben ilyen SP anomáliákat rögzítettek egy gránit tározóban. A cikk ezeket az anomáliákat vizsgálja és a hozzájuk kapcsolódó geokémiai és hidrodinamikai hátteret tárja fel. Elméleti kőzettani modelleket dolgoz ki, melyek az elektrokémiailag aktív ásványok által generált elektromotoros erők, valamint a kőzet-repedések anomália kialakuláshoz való hozzájárulásán alapszik.

EÖTVÖS L. GEOPHYSICAL INSTITUTE OF HUNGARY

THE OLDEST INSTITUTION FOR APPLIED GEOPHYSICS OFFERS THE LATEST ACHIEVEMENTS FOR GROUND-WATER PROSPECTING and ENVIRONMENTAL PROTECTION

The most often occurring demands:

- local geophysical measurements for the water supply of small communities by a few wells
- regional geophysical mapping to determine hydrological conditions for irrigation, regional agricultural development,
- large-scale exploration for the water supply of towns, extended areas i.e. regional waterworks,
- determination of bank storage of river terraces, planning of bank filtered well systems,
- thermal water exploration for use as an energy source, agricultural use or community utilization,
- cold and warm karst water prospecting,
- water engineering problems, water construction works

Field work with ELGI's 24-channel portable seismograph

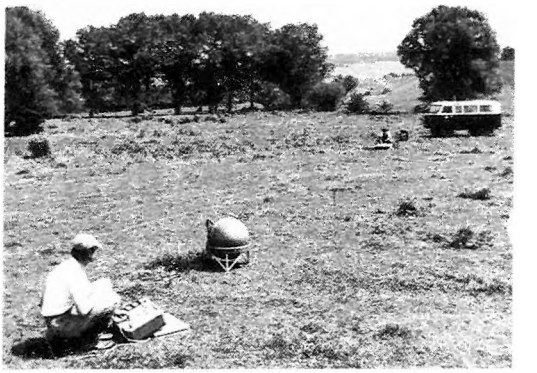

The Maxi-Probe electromagnetic sounding and mapping system – produced under licence by Geoprobe Ltd. Canada – is an ideal tool for shallow depths, especially in areas where seismic results are poor or unobtainable

ELGI has a vast experience in solving problems of environmental protection such as control of surface waters, reservoir construction, industrial and communal waste disposal, protection of surface and ground water etc. ELGI's penetrologger provides in-situ information – up to a maximum depth of 30 m – on the strength, sand/shale ratio and density without costly drilling.

ELGI offers contracts with co-operating partners to participate in the whole complex process of exploration–drilling–production.

For further information ask for our booklets on instruments and applications. Let us know your problem and we will select the appropriate method and the best instrument for your purpose.

Our address: ELGI POB 35. Budapest, H–1440. HUNGARY
Telex: 22-6194 elgi h